The dielectric response of chloromethylsilyl and dichloromethylsilyl dipolar rotors on fused silica surfaces

2002 Nanotechnology 13 533

(http://iopscience.iop.org/0957-4484/13/4/317)

INSTITUTE OF PHYSICS PUBLISHING NANOTECHNOLOGY
Nanotechnology **13** (2002) 533–540 PII: S0957-4484(02)34064-9

The dielectric response of chloromethylsilyl and dichloromethylsilyl dipolar rotors on fused silica surfaces

Laura I Clarke[1], Dominik Horinek[2], Gregg S Kottas[2], Natalia Varaksa[2], Thomas F Magnera[2], Tanja P Hinderer[1], Robert D Horansky[1], Josef Michl[2] and John C Price[1]

[1] Department of Physics, University of Colorado, Boulder, CO 80309-0390, USA
[2] Department of Chemistry and Biochemistry, University of Colorado, Boulder, CO 80309-0215, USA

Received 20 February 2002, in final form 26 June 2002
Published 26 July 2002
Online at stacks.iop.org/Nano/13/533

Abstract
We have measured the dielectric response of monolayer films of surface mounted chloromethyl- and dichloromethylsilyl dipolar rotors on fused silica at frequencies in the 1 kHz range and temperatures from 4 to 300 K. The torsional potentials, calculated from molecular mechanics, show an asymmetrical three-fold barrier to rotation with a barrier height sufficient to hinder motion of the rotor at experimental temperatures. A broad distribution of barrier heights is observed experimentally, consistent with calculated results showing that the intrinsic barrier of the rotor is modified by interactions with the underlying substrate. For a series of samples with differing concentrations of the rotor, the observed signal strength varies in proportion to the rotor coverage measured by Auger spectroscopy; however, the absolute strength of the signal is about three times larger than expected.

1. Introduction

Molecular rotors [1] are a fundamental element of molecular scale machinery [2–4]. Arrays of surface mounted molecular rotors with electric dipole moments are of particular interest because rotor–rotor interactions can be controlled and even designed to yield specific behaviour, such as ferroelectricity. Disordered two-dimensional arrays of dipolar rotors are predicted to form a glass phase [5, 6], while ordered arrays yield either ferroelectric or antiferroelectric ground states, depending on the lattice type. Arrays of dipolar rotors with vertical axes have been reviewed by Rozenbaum *et al* [7]. Two-dimensional arrays of adsorbed molecules without a dipole moment have been shown to have orientationally ordered phases [8–10]. In the present work, we study disordered two-dimensional arrays of covalently attached dipolar rotors. Each rotor has a permanent in-plane electric dipole moment, so the torsional motion of the rotor can be directly probed using dielectric spectroscopy with an externally applied electric field in the substrate plane. We access both the dilute limit, where rotors are non-interacting, and the high density limit, where a glass phase is expected.

For our experiments, we have used chloromethyltrichlorosilane to grow a two-dimensional array of surface mounted dipolar rotors. Monolayer thin films grown from alkyltrichlorosilanes have been widely studied [11, 12] and methyltrichlorosilane can be used to grow monolayers on fused silica from gas or liquid phase [13]. When chloromethyltrichlorosilane reacts with a fused silica surface, a chloromethylsilyl [$ClCH_2$–Si(O–)$_3$] rotor is formed. When the oxygen feet of the chloromethylsilyl are immobilized, the chloromethyl group, which has an in-plane component of the electric dipole moment of about 2 Debye (D), can still rotate, constrained by a barrier to rotation. Here, the barrier to rotation results from the intrinsic rotational potential of the attached molecule as well as interactions with the substrate. Our results below show that the chloromethylsilyl rotor on a fused silica surface has an asymmetrical three-fold barrier to rotation with barrier heights of a few kcal mol^{-1}. We study hindered rotation where the torsional barrier is much greater than either the thermal energy or the coupling energy between the dipole and an electric field. In this case, the molecules do not saturate under the presence of the electric field, but their random alignment is perturbed to produce a net polarization. The rotational barriers

serve to slow the response of the molecules into the dielectric spectroscopy range as the temperature is lowered. Due to the fact that the dipole moment of the rotor is small and the effect of the electric field is a perturbation of the random motion, we perform sensitive dielectric measurements, with a resolution of a few parts per million, in order to detect the motion of the rotors.

2. Experimental details

2.1. Sample preparation and characterization

Dielectric samples were prepared by growing silane thin films on fused silica substrates patterned with interdigitated gold electrodes. The electrodes were fabricated using standard UV lithography on a fused silica wafer coated with ∼200 nm of gold with ∼10 nm of titanium as an adhesion layer. Excess metal was removed by etching with KI/I_2 (gold) and then with HF (titanium). The resulting electrodes had a digit width and spacing of 10 μm and a digit length of 1 mm. Each device had 25 finger pairs and ∼1 pF capacitance. Silver epoxy was used to attach fine silver wires to the gold contact pads of the device.

As shown in table 1, two types of samples were grown: 'mixed monolayer' and '*in situ*'. For the mixed monolayer samples, chloromethyltrichlorosilane, methyltrichlorosilane and dichloromethyltrichlorosilane were purchased from Aldrich and used without further purification. After transfer to Schlenck tubes in a glove box, the trichlorosilanes were degassed using the freeze–pump–thaw technique. Substrates were cleaned by successive washing with acetone, chloroform and methanol, and dried in a stream of argon between washes. The monolayer films were grown by evacuating substrates to 10^{-5} Torr, disconnecting the vacuum pumps, and then opening a Schlenck tube containing the trichlorosilanes, which were maintained at either 0 or −78 °C. For each growth, both a fused silica wafer patterned with electrodes and a silicon substrate with native oxide were used. Ellipsometry and Auger spectroscopy measurements were performed on the silicon substrate. Auger measurements on fused silica, fused silica with electrodes and silicon with native oxide showed the same results.

In situ samples were grown inside the cryostat using a similar procedure except the resulting samples were neat instead of mixed. The trichlorosilanes were prepared as above. After initial measurements on a fused silica substrate, patterned with electrodes but with no film, the cryostat was warmed to room temperature and the sample exposed to chloromethyltrichlorosilane. In this case, the Schlenck tube was at room temperature and opened to the evacuated environment for a few seconds at a time. After one or more doses, the tube was closed and after approximately 30 min, the sample space was re-evacuated, cooled and measurements were resumed.

To measure the thickness of the mixed monolayer thin films, ellipsometry measurements were made on the silicon substrate before and after exposure to the rotor molecules using a Rudolph AutoEL ellipsometer, at a wavelength of 650 nm and an angle of 70°. An average value from at least five points on the surface was used to determine the thickness. The refractive index of films grown from alkyltrichlorosilanes has been estimated [17] to be close to 1.46; the value for fused silica. This value was used to model both the intrinsic SiO_2 layer on the silicon wafer before film deposition and the rotor-covered surface after deposition. A multi-angle, multiwavelength Woollam VB 250 VASE ellipsometer was also used on some samples and the results agreed with those obtained above.

Auger spectroscopy measurements, taken with a Perkin–Elmer PHI 600 scanning Auger multiprobe, were used to confirm and quantify the chlorine on the surface of the samples, giving a measure of the number of rotors. Care was taken to minimize damage to the thin organic films by using low beam currents (5–10 nA) and short measurement times (1–2 min). After each measurement, the electron beam was moved to a new position on the sample, and an average of the results from approximately ten points on the surface was used to determine the quoted value.

2.2. Dielectric measurements

The dielectric measurements were taken in a homemade cryostat over the range 4–300 K. The sample was attached to a copper block with thermally conducting vacuum grease and evacuated to 10^{-5} Torr. A Lakeshore 331 temperature controller was used for temperature measurements and control with a silicon diode and a resistive heater attached to the copper block. Dielectric relaxation measurements utilized a capacitance bridge to measure both the capacitance and dissipation factor, $\tan(\delta)$. Measurements were taken at 1 and 10 kHz with an rms amplitude of 5 V applied across the 10 μm spacing of the electrodes. Both a Gen–Rad 1615-A bridge with a lock-in amplifier used as a balance detector and a fully automated Andeen–Hagerling 2700A bridge were used for dissipation measurements with five to ten data points taken at each temperature after a settling time of 10–20 min. The noise contribution of the instruments to the dissipation factor measurements may be estimated from the scatter in the points at each temperature, commonly $1–2 \times 10^{-6}$, as shown in the inset in figure 5. Due to fact that the magnitude of the raw dissipation factor is very low (always less than 2×10^{-4}), the absolute accuracy required in the dissipation factor measurement is not high. The stated accuracy of the Gen–Rad instrument is 2×10^{-5} in loss due to the dissipation of the internal capacitance standards in the bridge, while the Andeen–Hagerling instrument has lower internal losses. These effects can only cause a temperature independent offset in the data. For samples measured with both experimental apparatus, the results agreed.

2.3. Molecular dynamics simulations and calculations

Computer simulations utilized either a model of an amorphous SiO_2 surface or of the (100) surface of crystalline quartz. The model surfaces were approximately the same size; for instance, the glass surface area was 5.5×5.5 nm^2 with approximately 3500 Si and O atoms. On the glass surface rotors were attached by removing a hydroxyl group from the surface and bonding to the free Si valence. To assess the variety of molecular environments available on the amorphous surface, calculations were performed with the rotor molecule

Table 1. A summary of the five samples, including sample type, the relative coverage measured by Auger spectroscopy, and the relative coverage from fitting the dielectric data without accounting for non-responsive rotors.

Sample no	Sample type	Auger relative coverage	Dielectric relative coverage (without suppression)
1	Chloro mixed	0.21 ± 0.04	0.25 ± 0.06
2	Chloro *in situ*	0.28 ± 0.12	0.25 ± 0.13
3	Chloro mixed	0.88 ± 0.24	0.09 ± 0.03
4	Dichloro mixed	0.06 ± 0.02	0.10 ± 0.01
5	Dichloro mixed	0.07 ± 0.01	0.05 ± 0.02

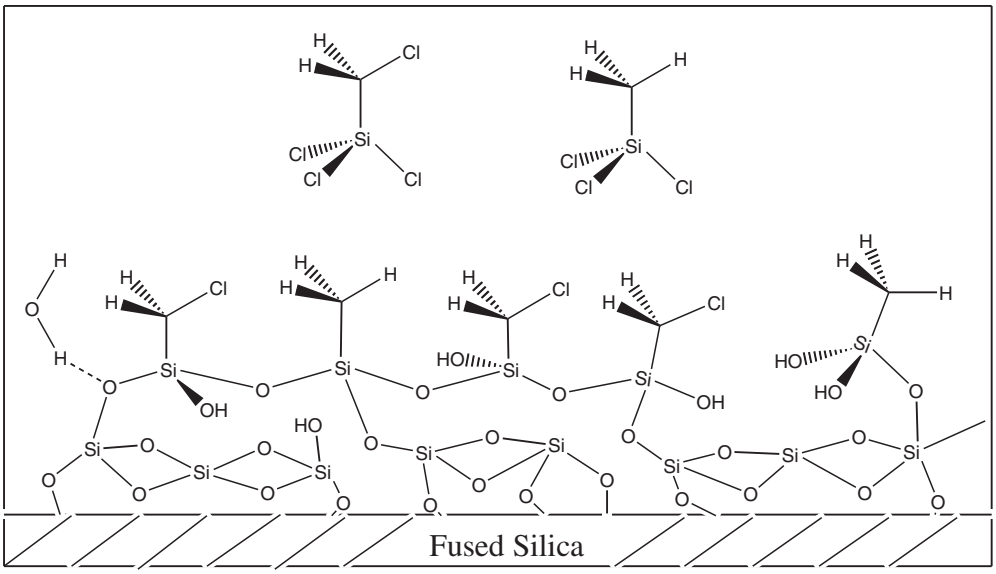

Figure 1. The attachment of chloromethylsilyl and methylsilyl to a fused silica surface. The trichlorosilanes react with adsorbed water and hydroxyl groups on the surface, as well as neighbouring molecules, forming HCl and water as by-products.

at nine different sites on the fused silica. Attachment to the crystal surface was achieved by replacing three hydroxyl groups by a $ClCH_2–Si(O–)_3$ unit to obtain a rotor with the axis of rotation approximately perpendicular to the surface, as shown in figure 2(a).

A classical molecular dynamics program [14] using the universal force field (UFF) [15] was used for calculations. Partial atomic charges were obtained by the method of charge equilibration [16], except for the partial charges of the rotor group, which were calculated by the density functional theory (B3LYP/6-31G*). The classical equations of motion were solved using the velocity verlet integrator. Trajectories were calculated at 100, 200 and 300 K for 1.2 ns with a time step of 1 fs. In addition to dynamics calculations, torsional potentials were obtained for rotors on the surfaces by constraining one of the three Cl–C–Si–O dihedral angles and optimizing all remaining degrees of freedom using a constrained truncated Newton optimizer. This procedure yielded the minimum energy conformation with the energy calculated in steps of 5°.

3. Results

3.1. Sample preparation and characterization

For the mixed monolayer samples, ellipsometry measurements taken before and after deposition showed an increase in height of 3–5 Å, which is consistent with a monolayer based upon known bond lengths and angles [17]. For exposure times of 0.5–5 min, the surface appeared to saturate at a monolayer of coverage. Although ellipsometry indicates that the average value of the film thickness is consistent with monolayer coverage, it is possible that some island growth (along with patches without film) could be present. Atomic force microscopy (AFM) studies in our laboratory of films grown from trichlorosilanes using the same technique show no islands, but the resolution of such measurements is of the order of nanometres, larger than the expected thickness of one monolayer.

For the mixed monolayer samples, methylsilyl was used as a non-polar diluent to control the dipole coverage, as illustrated in figure 1. In this case, a mixture of methyltrichlorosilane and either dichloromethyl- or chloromethyltrichlorosilane was used for film preparation. Due to the fact that both the vapour pressure and reactivity of the molecules differ, an independent measure of coverage was obtained by Auger spectroscopy. A monolayer sample of chloromethyl rotors (1:0 chloromethyl:methyl) showed 0.89 ± 0.09 as the ratio of the area under the Cl peak to the area under the Si peak (Cl/Si ratio). For samples with an unknown chloromethyl:methyl mixture, the Cl/Si ratio was normalized by this value to determine the chloromethyl fraction of full coverage, which we refer to as the relative coverage. A similar analysis was performed for the dichloromethyl samples. For each coated substrate, measurements were taken at several

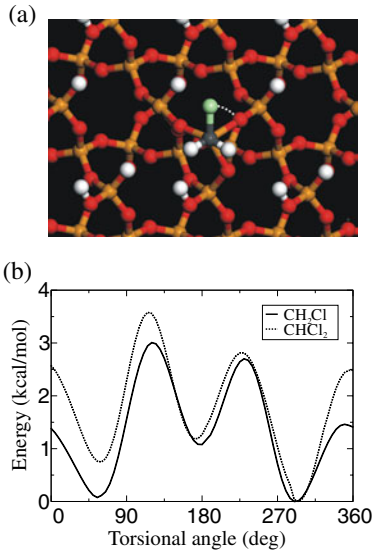

Figure 2. (a) A ball and stick model of a chloromethyl rotor attached to the (100) surface of crystalline quartz where the gold-coloured atoms are silicon, red oxygen, white hydrogen, grey carbon and green chlorine. The torsional angle of the rotor is indicated. The view is looking down on several crystal planes and thus the hydroxyl oxygen atoms appear overcoordinated. (b) Calculated torsional potentials for chloromethyl and dichloromethyl rotors attached to the crystalline quartz surface.

points on the surface and the results were averaged. To determine the resolution of the Auger results, we also tested both a bare silicon wafer and a methyl control film (0:1 chloromethyl:methyl), which should show no chlorine peaks. Our noise limit, the Cl/Si ratio found in this case, corresponded to a relative coverage of 0.07 for chloromethyl rotors or 0.04 for dichloromethyl rotors. The relative coverage from Auger spectroscopy for the five samples discussed here is shown in table 1. For mixed monolayer samples, relative coverage less than one is expected even for a monolayer film; however, the *in situ* samples were fabricated without a diluent (neat) and thus a relative coverage of less than one is indicative of sub-monolayer coverage.

In order to correlate the Auger results with the dielectric data, it is helpful to determine the actual number of chloromethyl groups on the surface in addition to the relative coverage. We have measured the surface density of a monolayer grown on fused silica from 3-cyanopropyltrichlorosilane, which should be similar to the density of our films. For that experiment, a series of monolayer Langmuir–Blodgett films of 5, 10, 15, 20-tetra (4-pyridyl)–21H, 23H-porphyrin (TPyP) were formed on the water subphase, compressed, and transferred to fused silica substrates with a transfer ratio close to 1. Auger spectroscopy on the films provided a calibration plot of the relative intensity of the Auger nitrogen signal versus the surface density of TPyP and thus a conversion ratio was obtained. TPyP was chosen for this calibration because it formed well defined surfaces under compression, was resilient to the electron beam in the Auger spectrometer and contains 8 nitrogen atoms mol^{-1}, providing a large signal. The calibration from TPyP was used to interpret Auger spectroscopy data from a monolayer film of 3-cyanopropylsilyl that was grown on fused silica from a 1 mM solution in hexanes. A surface density of 5–7 $\times$ 10^{18} m^{-2} (15–20 $Å^2$ mol^{-1}) was found, which is consistent with the values in the literature for films grown from trichlorosilanes [17, 18].

3.2. Molecular dynamics simulations and calculations

The intrinsic barrier for the chloromethyl rotor can be estimated from the torsional potential of $ClCH_2$–$Si(OH)_3$ (hydroxyl groups in the gauche conformation) which is symmetrical with a calculated barrier height of 1.8 kcal mol^{-1}. The calculated torsional energy potential for a chloromethyl rotor placed on the crystalline quartz surface is shown in figure 2(b). An asymmetrical three-fold potential barrier is observed with barrier heights in the 1.5–3.0 kcal mol^{-1} range. The asymmetry of the potential indicates that the non-bonding interaction with the surface is superimposed on the intrinsic torsional potential barrier. For the dichloromethyl rotors, the calculated intrinsic barrier is 2.7 kcal mol^{-1}. When placed on the crystalline quartz surface, the torsional potential, also shown in figure 2(b), has a similar range of barriers as the chloromethyl rotor but with slightly higher barrier values.

When calculations are performed for rotors placed on the amorphous fused silica surface, the system becomes inhomogeneous. For the nine sites on which the chloromethyl molecule was placed, a broad distribution of well and barrier energies was observed, and a histogram of the barrier heights is shown in figure 3. Here only about one-third of the barriers fall into the 1.5–3.0 kcal mol^{-1} range. The width of the distribution indicates that the non-bonding interaction with the surface can be much greater for the amorphous surface than the crystalline quartz surface. In particular the angle between the axis of the rotor and the surface has a substantial effect on the size of the surface interactions. In order to explore the lack of homogeneity observed for the calculated amorphous surface, we re-calculated the torsional potentials omitting different parts of the interactions between the rotors and the surface. Neglecting both the van der Waals and Coulomb interactions for atoms separated by more than three bonds, the resulting barrier distribution is close to the crystal data. The removal of only the electrostatic interactions indicates that the van der Waals short-range repulsion often is the biggest contribution but the electrostatic influence cannot be disregarded. For instance, when we calculated torsional potentials with the rotor partial charges derived by different quantum chemical methods, we observed barriers that varied by as much as 2 kcal mol^{-1}.

In all simulations, the angular motion of the rotor can be described as a libration in one of the three minima of the torsional potential, combined with jumps from one minimum to another. This is illustrated in the rotor angle versus time plot from a simulation at 300 K shown in figure 4(b) for the potential shown in figure 4(a). The eigenfrequency of the libration was obtained by two separate procedures: first, we fitted a harmonic potential to the lowest minimum of the torsional potential of each of the chloromethyl rotors and calculated the frequency of this harmonic vibration. Here, the moment of inertia used was derived from the equilibrium geometry of the rotor group as obtained from the torsional barrier calculations. The frequencies obtained range from 960 to 1840 GHz with seven of the nine falling between

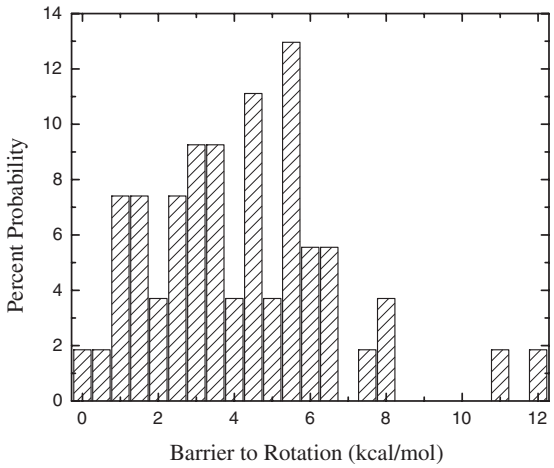

Figure 3. Barrier height distribution from the calculated torsional potentials for chloromethyl rotors placed on nine sites on the amorphous fused silica surface.

1300 and 1550 GHz. The dichloromethyl frequencies varied from 760 to 1860 GHz. As a second approach, we obtained the eigenfrequencies by Fourier transform of the rotor angle versus time plots. The frequency domain data showed a distinct peak for every rotor with a frequency that did not depend on temperature over the measured range. The observed eigenfrequencies are consistently 100–200 GHz lower than the ones from the fit. This is a reasonable agreement given that the simulations at non-zero temperatures sample a larger portion of the potential energy surface and that the curvature of the potential may not be well fitted by the harmonic approximation.

With respect to the hopping motion between the wells, the relative occupancy of a simulated rotor at each angle is calculated from figure 4(b) and shown as (c). Due to the fact that the well energies are not degenerate, the simulations show that the motion of the rotor is dominated by hopping between the two lowest energy wells (the two wells whose minima have the lowest absolute energy). This effect increases as the temperature is reduced and thus we expect that most rotors can be treated as effective two-level systems. In the extreme case, some rotors will have too great a difference between the absolute well energies to allow significant occupancy in any but the lowest energy well and will be non-functioning or 'frozen' at experimental temperatures.

3.3. Dielectric measurements

A characteristic plot of dissipation factor versus temperature for a methyl control silane film [0:1 chloromethyl:methyl] on fused silica is shown as the inset to figure 5. At each temperature, five data points, taken in 60 s intervals, are displayed. The decrease in $\tan(\delta)$ as the temperature increases has been observed in bulk samples of fused silica and is attributed to hydroxyl groups (OH) in the bulk, with the magnitude of the slope increasing with increasing OH concentration [19]. In our case, this slope and the absolute magnitude of the dissipation factor vary slightly from sample to sample and thus a straight line has been subtracted from the data in the main figure so that the structure of the dissipation factor can be seen. Characteristic adjusted 1 kHz data for a methyl

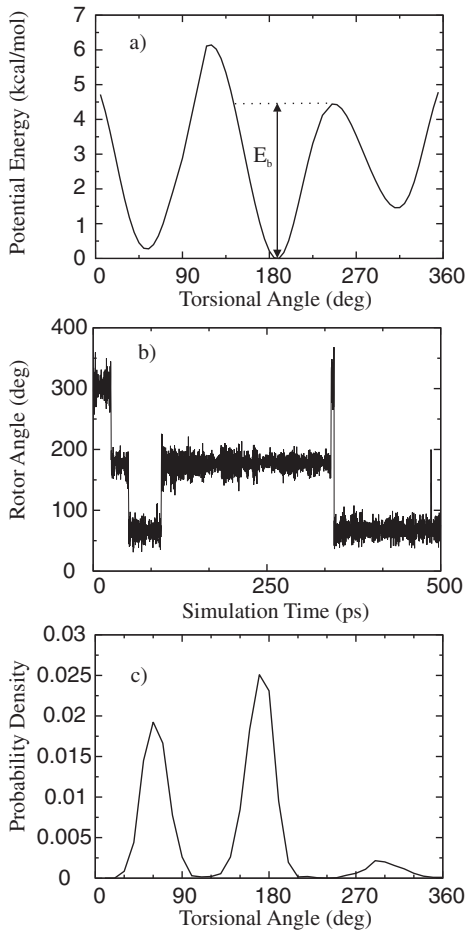

Figure 4. (a) Calculated torsional potential curve for a chloromethyl rotor on the amorphous fused silica surface. The barrier to rotation for hopping from the centre to the right well is indicated. (b) Rotor angle versus simulation time at 300 K without an applied electric field. An angular change of 360° corresponds to a full turn. (c) Probability density versus rotor angle as calculated from (b).

control sample, a bare sample, chloromethyl samples nos 2 and 3 and dichloromethyl sample no 4 are shown in figure 5. For sample no 2, the two curves shown reflect the uncertainty due to the subtraction of the straight line. The dissipation factor of all samples shows a 'bump' at low temperatures, which coincides in position and amplitude with a feature seen in bulk measurements on fused silica [19, 20]. Because this feature is present in all samples and appears to be related to bulk effects, we have adjusted the dissipation factor by subtracting an appropriate control from each data set before subsequent analysis. For mixed monolayer samples, the methyl control sample is used for this purpose. For the sample grown *in situ* in the cryostat, the dissipation factor after exposure to the molecules is compared with curves taken before exposure. As illustrated in figure 5, all data from samples with dipolar rotors showed structures not seen in the control measurements. For each sample, these structures varied in shape and amplitude as the temperature was cycled. The upturn at high temperature shown in some sweeps is the tail of a large peak at $\sim$200 K, which varies from sample to sample and appears to be due to adsorbed water.

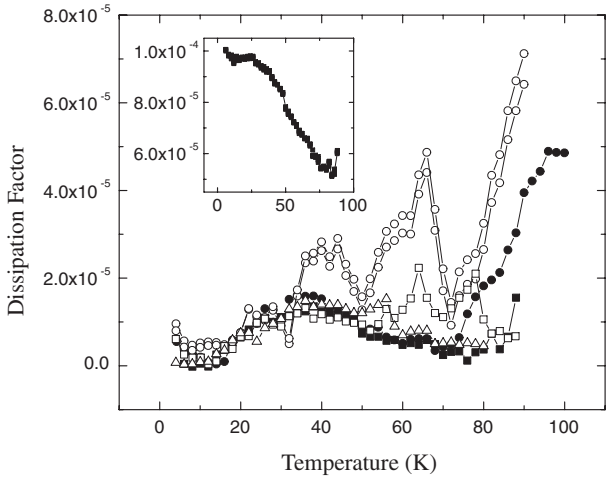

Figure 5. 1 kHz dissipation factor, where a straight line has been subtracted from each dataset, for: a bare fused silica sample (filled circles), a full coverage film of methyl control molecules (filled squares), chloromethyl sample no 2 (open circles), chloromethyl sample no 3 (open triangles) and dichloromethyl sample no 4 (open squares). An average value of several points is plotted for each temperature where the spread in the points was 1–2 $\times$ 10^{-6} in the raw data. The data for sample no 2 were taken with slightly different settings on the capacitance bridge and the spread of the points in this case was about 5 $\times$ 10^{-6}. For sample no 2, the two sweeps shown reflect the uncertainty due to the subtraction of the line. The inset shows raw data from the methyl control sample. Five points, taken at 60 s intervals, are plotted for each temperature.

4. Analysis and discussion

4.1. Basic behaviour of the system

Given the energy scales in the system, namely that the barrier to rotation, $E_{barrier}$, is much greater than either the thermal energy or the coupling energy between the dipole and the field, we expect that the dominant mechanism for dipole relaxation will be thermally activated hopping. In this case, the hopping rate, $1/\tau$, is given as [21]

$$\frac{1}{\tau} = \omega_0 \exp\left(\frac{-E_{barrier}}{kT}\right) \tag{1}$$

where ω_0 is an attempt frequency, which we take as equal to the angular libration frequency calculated from the simulations, $\sim 9 \times 10^{12}$ rad s^{-1}. As discussed in section 3, we consider each rotor as an effective two-level system. The relaxation rate of the rotor will be the sum of the hopping rates into and out of the lowest energy well. From the calculated torsional potentials, we find that for most rotors, the hopping rates vary sufficiently so that hopping over the lowest barrier between the two lowest energy wells determines the dynamics of the rotor at experimental temperatures. Thus, one effect of the non-degeneracy of well energies is that a single barrier to rotation dominates the relaxation rate of the rotor.

The relaxation rate of the rotors is experimentally accessed by measuring the dissipation factor which, for a single exponential relaxation, is given by the Debye form [21]

$$\tan(\delta) = \frac{C}{C_0}\frac{\omega\tau}{(1+\omega^2\tau^2)} \tag{2}$$

where ω is the frequency of the applied field, C_0 is the capacitance of the electrodes and C is the effective capacitance due to the rotor response. The contribution of each rotor to the polarizability is given by

$$\alpha = p_0\left[\frac{p_0}{2kT}\right]\mathrm{sech}^2\left(\frac{B}{2kT}\right) \tag{3}$$

where p_0 is the intrinsic in-plane dipole moment and the bracketed term includes the Curie factor and angular averaging. B is the difference in energy between the two lowest energy wells and the sech^2 term takes into account the inability of the field to align a rotor against the potential difference of the wells [22]. Considering the geometry of the interdigitated capacitors, the capacitance due to the rotor response is then given by

$$C = \frac{d}{L}\frac{\alpha}{a^2} = n\frac{\alpha}{L^2} \tag{4}$$

where L is the distance between fingers, d the total meander length, $1/a^2$ is the surface density of the rotors and n the number of rotors.

4.2. Effective barrier distributions from experimental results

For a single barrier to rotation (if each molecule has the same rotational potential with three identical wells), we expect a single peak in the dissipation factor at the temperature where the relaxation rate of the rotors equals the frequency of the applied field. The experimental observation of both multiple features and peaks that are broader than predicted is consistent with the calculated result that the rotors are not homogeneous on the surface. This observation can be quantified by fitting the observed dissipation factor with a superposition of individual barrier peaks (equation (2)), as shown in figure 6. For each individual peak, the prefactor, C, is proportional to the number of rotors contributing to that peak, n, according to (4) while the time constant, τ, is related to the barrier height through (1). The barrier height distribution obtained from the fits obviously reflects only those rotors that contribute to the dielectric signal in the temperature range measured. Furthermore, because the data provide no independent information about the distribution of well energies, B, we have set the sech^2 term in (3) to one in obtaining the effective barrier distribution.

In fact, the non-degeneracy of well energies will affect the dielectric response of the rotors. As the energy difference between the two lowest energy wells is increased, the response of the rotor is suppressed by the sech^2 term in (3). In particular, rotors with B in excess of a few times kT ($\sim$0.5 kcal mol^{-1}) at the temperature where a signal would be observed (T such that $\omega\tau = 1$) are strongly suppressed. Using B values from the computational results, we estimate that for a uniform distribution, only about one-third of the rotors on the crystalline surface and one-eighth of the rotors on the amorphous surface would contribute to the dielectric signal. This gives a range of expected suppression values. As we discuss below, the size of the observed experimental signal is larger than expected in either case, but in better agreement with the results from the crystalline surface.

The effective chloromethyl rotor barrier distribution, obtained from fitting dielectric data from three samples, is shown as figure 7. The individual barrier distributions for each

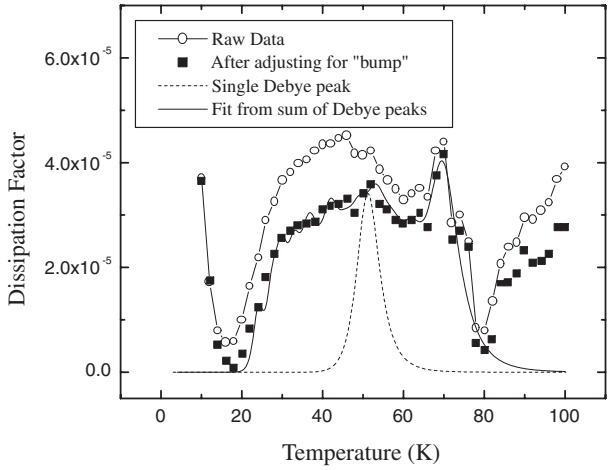

Figure 6. A demonstration of the fitting procedure. The curves are raw data with a straight line subtracted (open circles), data corrected for the bulk 'bump' (filled squares), a single Debye relaxation peak (dotted curve) and a fit, the sum of many single peaks, (solid curve) for sample no 1 at 1 kHz.

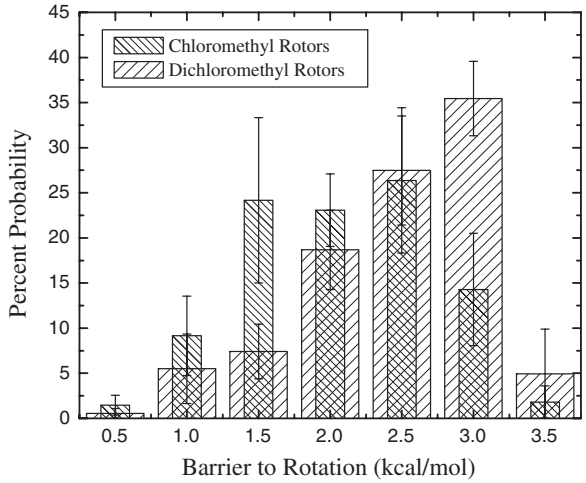

Figure 7. The average barrier height distribution for chloromethyl and dichloromethyl rotors inferred from fits to the dissipation factor. The error reflects the spread of values among the different samples.

of the three samples are shown in figure 8. For each sample, the value is an average of several runs, with different applied frequencies and differing temperature sweep directions. Also shown in figure 7 is the effective dichloromethyl barrier distribution, an average of the two samples.

4.3. Comparison of experimental and computational results

The values and breadth of the experimental barrier distributions shown in figure 7 are consistent with the calculated torsional energy potentials on the crystalline quartz surface with about 75% of the experimental signal falling in the range 1.5–3.0 kcal mol^{-1}. With respect to the molecular modelling, the crystalline quartz and amorphous fused silica systems represent two limiting cases of the surface topography. The crystalline surface is flat and the rotor is attached perpendicularly to the surface. The inhomogenity found in the potentials is therefore intrinsic to SiO_2, and, within the errors

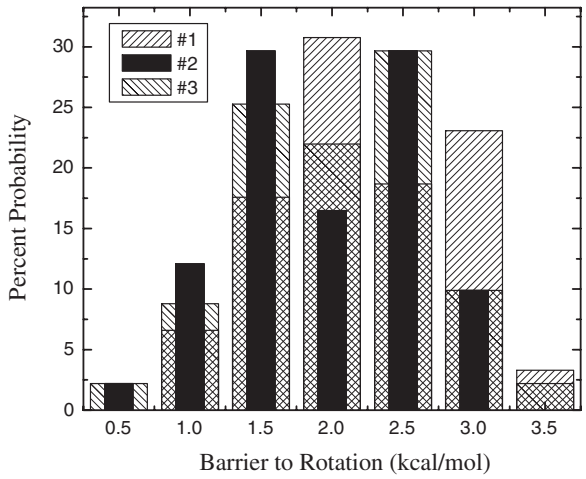

Figure 8. The barrier height distributions inferred from the fits to the dissipation factor for the three chloromethyl samples.

of the calculation, we cannot expect to obtain sharper torsional barrier distributions. The experimental results are consistent with this hypothesis, showing similar values for the barrier heights but a broader distribution. In contrast to the crystalline quartz, the calculated glass surface is very uneven and the rotor axle orientations are widely distributed. Comparing the experimental barrier distribution to these two limiting cases shows that the actual surface environment of the rotors does not appear to be as disordered as the calculated glass surface would indicate.

4.4. Comparison of dielectric and Auger spectroscopy coverage

From the fits of the experimental data, we also obtain the size of the total observed signal and thus determine the relative coverage of rotors. This value can then be compared with the relative coverage measured by Auger spectroscopy. Using the amplitude of the single barrier peak fits, the temperature at which they occur and an estimate of the in-plane contribution of the dipole moment as 2.0 D, we estimate the number of rotors with each barrier from (4). (The dipole moment of chloromethyl and dichloromethyl rotors is identical.) Here we have used the known geometrical values of the capacitor: C_0, L, and d, and $\alpha = p_0^2/2kT$. Summing the number of rotors over all observed barriers, we obtain an estimate of the total number or alternatively, the surface density of rotors. Comparing this value with our estimate for maximum full coverage surface density, 7×10^{18} m^{-2}, we obtain the relative coverage values shown in the fourth column of table 1, which are in apparent agreement with the estimates obtained from Auger spectroscopy. However, as discussed above, the calculated results indicate that at most one-third of the rotors should be responsive to the dielectric measurements. We conclude that the signal obtained experimentally is at least three times larger than expected.

For samples nos 1, 2, 4, and 5, the estimates from the electrical measurements give coverages proportional to those obtained from Auger spectroscopy. However, for sample no 3, the observed dielectric response is much smaller, relative to the Auger coverage. We explain this result by considering the

interaction energy. For a pair of in-plane dipoles p_0 separated by a, we expect the maximum dipole–dipole interaction energy to go as

$$U \sim \frac{1}{4\pi\varepsilon_0}\frac{p_0^2}{a^3}. \tag{5}$$

For a dipole moment of 2.0 D and a surface density consistent with the coverage of sample no 3, U is greater than 300 K. We consider this sample to be a dipolar glass. The dielectric relaxation that we observe for sample no 3 probably results from the less dense portions of the film and cannot be predicted from the total coverage measured by Auger. For other samples, the dielectric signal scales with the observed Auger coverage indicating they are sufficiently dilute so that dipole–dipole interactions are not important.

5. Conclusions

We have measured the dielectric response of chloromethyl and dichloromethyl rotors on a fused silica surface. The rotational barrier distribution observed is quite broad as predicted by force field calculations. The coverage estimated from the electrical data is proportional to that measured by Auger spectroscopy for samples that are sufficiently dilute. We observe no significant difference between the barrier distributions measured for chloromethyl samples with a dilute mixed monolayer, a glassy mixed monolayer or a sub-monolayer coverage. We expect that a narrow distribution of barrier heights would be observed with molecules which are less sensitive to surface interactions. This should be the case if the rotary portion of the molecule is farther from the surface, i.e. if the molecule is taller. Several rotors of this type are currently being explored.

Acknowledgments

This work was supported by the US National Science Foundation under grant no 98-71917 and the US Army Research office under grant no DAAD19-01-1-0521 (DURINT). DH thanks the Alexander von Humboldt Foundation for a Feodor Lynen fellowship. The authors wish to thank Boris Pinkhasov, Michael Varney, Daniel Dessau, and Charles Rogers for help with Auger spectroscopy.

References

[1] Vacek J and Michl J 2001 *Proc. Natl Acad. Sci. USA* **98** 5481
[2] Gimzewski J K, Joachim C, Schlittler R R, Langlais V, Tang H and Johannsen I 1998 *Science* **281** 531
[3] Koumura N, Zijlstra R W J, van Delden R A, Harada N and Feringa B L 1999 *Nature* **401** 152
[4] Bermudez V, Kapron N, Gase T, Gatti F G, Kajzar F, Leigh D A, Zerbetto F and Zhang S 2000 *Nature* **406** 608
[5] Rozenbaum V M and Ogenko V M 1991 *J. Electron Spectrosc. Relat. Phenom.* **57** 279
[6] Rozenbaum V M and Ogenko V M 1988 *Sov. Phys.–Solid State* **30** 1753
[7] Rozenbaum V M, Ogenko V M and Chuiko A A 1991 *Sov. Phys.–Usp.* **34** 883
[8] Kim K and Sullivan N S 1997 *Phys. Rev.* B **55** R664
[9] Chacon E and Tarazona P 1989 *Phys. Rev.* B **39** 7111
[10] Marx D, Sengupta S and Nielaba P J 1993 *J. Chem. Phys.* **99** 6031
[11] Ulman A 1996 *Chem. Rev.* **96** 1533
[12] Fadeev A Y and McCarthy T J 2000 *Langmuir* **16** 7268
[13] Tripp C P and Hair M L 1992 *Langmuir* **8** 1961
[14] Vacek J and Michl J 1997 *New J. Chem.* **21** 1259
[15] Rappe A K, Casewit C J, Colwell K S, Goddard W A III and Skiff W M 1992 *J. Am. Chem. Soc.* **114** 10 024
[16] Rappe A K and Goddard W A III 1991 *J. Phys. Chem.* **95** 3358
[17] Ulman A 1991 *An Introduction to Ultrathin Organic Films: From Langmuir–Blodgett to Self Assembly* (Boston, MA: Academic)
[18] Stevens M J 1999 *Langmuir* **15** 2773
[19] Mahle S H and McCammon R D 1969 *Phys. Chem. Glass* **10** 222
[20] Ozaki T, Ogasawara T, Kosugi T and Kamada T 1999 *Physica* B **263–4** 333
[21] McCrum N G, Read B E and Williams G 1967 *Anelastic and Dielectric Effects in Polymeric Solids* (New York: Dover) p 14
[22] Daniel V V 1967 *Dielectric Relaxation* (London: Academic) p 24